Letter

# Atomic-level precision creation and manipulation of interfacial Se chemisorbates in graphene/$WSe_2$ heterostructures

Mo-Han Zhang,[1,*] Fei Gao,[2,3,*] Aleksander Bach Lorentzen,[2] Ya-Ning Ren,[1] Ruo-Han Zhang,[1] Xiao-Feng Zhou,[1] Rui Dong,[1] Shi-Wu Gao,[4] Mads Brandbyge,[2] and Lin He[1,†]

[1]*Center for Advanced Quantum Studies, School of Physics and Astronomy, Beijing Normal University, Beijing 100875, China and Key Laboratory of Multiscale Spin Physics, Ministry of Education, Beijing 100875, China*

[2]*Department of Physics, Technical University of Denmark, 2800 Kongens Lyngby, Denmark*

[3]*Donostia International Physics Center (DIPC), 20018 Donostia-San Sebastián, Spain*

[4]*Beijing Computational Science Research Center, 100193 Beijing, China*

(Received 23 November 2023; revised 5 July 2024; accepted 8 July 2024; published 23 July 2024)

It has long been an ultimate goal to introduce chemical doping at the atomic level to precisely tune properties of materials. Two-dimensional materials have a natural advantage due to their high surface to volume ratio, but achieving this goal experimentally remains a huge challenge. Here, we demonstrate the ability to introduce chemical doping in graphene with atomic-level precision by controlling chemical adsorption of individual Se atoms, which are extracted from the $WSe_2$ that is underneath, at the interface of the graphene/$WSe_2$ heterostructures. Our scanning tunneling microscopy (STM) measurements, combined with first-principles calculations, reveal that individual Se atoms can chemisorb on three possible positions in graphene, which generate distinct pseudospin-mediated atomic-scale vortices in graphene. Furthermore, the chemisorbed positions of individual Se atoms can be manipulated by the STM tip, which enables us to achieve atomic-scale control of quantum interference of the pseudospin-mediated vortices in graphene. This result offers the promise of controlling properties of materials with atomic-level precision through chemical doping.

DOI: 10.1103/PhysRevB.110.L041405

Manipulating chemical doping with atomic-level precision would play a significant role in realizing the ultimate functional materials for electronics and optoelectronics devices. Two-dimensional (2D) materials facilitate a natural advantage for chemical doping at atomic-level precision because of the highly exposed surface [1,2]. Recently, different strategies have been developed to introduce chemisorbed atoms or atomic defects in graphene to tune its properties [3–21]. It has been demonstrated explicitly that even a single chemisorbed H atom can drastically modify the magnetic and electronic properties of graphene [7]. For instance, a single H atom adsorbed on graphene can result in a pseudospin-mediated atomic-scale vortex with angular momenta reflecting the Berry phase of graphene [16–18]. Although much effort has been made to introduce point defects in graphene [7,16–21], precisely controlling the chemisorption sites of individual atoms faces many challenges, not to mention controlling chemisorbed atoms at the interface.

In this Letter, we report a facile method to realize atomic-level precise doping in graphene through manipulating the chemisorption of individual selenium (Se) atoms at the interface of graphene/$WSe_2$ heterostructures. Our scanning tunneling microscopy (STM) measurements, supported by first-principles calculations, show that a single Se atom separated from $WSe_2$ can form bonds with graphene at three different sites, the A sublattice, the B sublattice and the carbon-carbon (C-C) bridge, which introduce distinct pseudospin-mediated atomic-scale vortices in graphene. By using the STM tip, we demonstrate the ability to manipulate the chemisorbed positions of individual Se atoms at the interface and further obtain their possible combinations with atomic-level precision. This enables us to explore quantum interference of the pseudospin-mediated atomic-scale vortices in graphene.

We chose the graphene/$WSe_2$ heterostructure because individual Se atoms can be extracted from the $WSe_2$ by a proper tip pulse, and further chemisorbed on graphene by forming the Se-C bonds [22,23]. Figure 1(a) schematically illustrates the process and a small voltage pulse, usually between 2 and 4 V, is used in our experiment. The structural integrity of the topmost graphene is retained because graphene has a larger elastic constant and the C-C bond in graphene is much stronger than the Se-W bond in the $WSe_2$ [23]. The STM has sufficient spatial resolution to characterize the interfacial Se-C chemisorption and the atomic Se defects beneath graphene, as demonstrated subsequently and in previous studies [24,25]. Figure 1(b) shows a representative result obtained in the experiment. The interfacial chemisorbed Se atom is shown as a bright protrusion that is about 2 nm away from the Se vacancy in the $WSe_2$ substrate, which exhibits three brilliant protrusions appearing as trigonal symmetry with a dark center (see Fig. S2 and the Supplemental Material (SM) Secs. 2 and 3 for more details [26]; also see Refs. [27–38]). Scanning tunneling spectroscopy (STS), i.e., $dI/dV$, measurements

*These authors contributed equally to this work.
†Contact author: helin@bnu.edu.cn

 

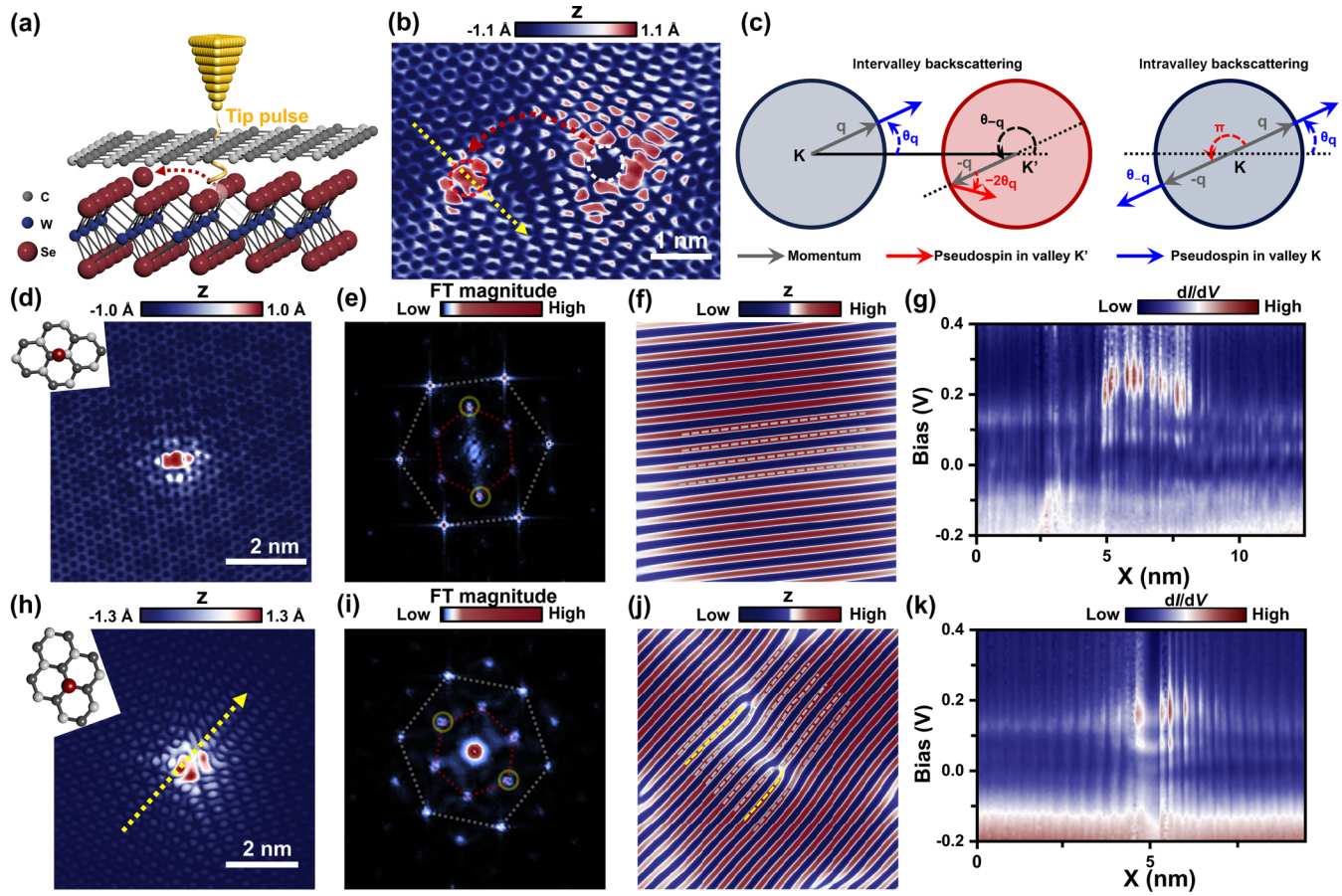


FIG. 1. (a) Schematics of a graphene/$WSe_2$ heterostructure after a tip pulse. The STM tip pulse creates a Se adatom and a Se vacancy in $WSe_2$. (b) STM topography of a graphene/$WSe_2$ heterostructure with a single Se atom chemisorbed on monolayer graphene (red dotted circle) and a Se vacancy in the $WSe_2$ substrate (white dotted circle). (c) The backscattering process in graphene. Intervalley backscattering leads to a rotation of $-2\theta_{\mathbf{q}}$ of the pseudospin. Intravalley backscattering rotates the pseudospin by $\pi$. (d), (h), Topography STM images of a Se adatom under the C-C bridge and the carbon atom of the graphene, respectively. The insets present atomic structures. (e) Modulus of the FT of the image in the red square of panel (d). (i) Modulus of the FT of the image in panel (h). In panels (e), (i), the outer hexangular spots and inner bright spots correspond to the reciprocal lattice of graphene and the interference of the intervalley scattering, respectively. (f), (j) FT-filtered images enclosed by yellow circles in (d), (i). (g), (k) Spatially resolved contour plots of $dI/dV$ spectra along the yellow arrows in (b), (h), respectively.

of the Se vacancy show two localized electronic states at about 0.7 eV (see Fig. S2 in the SM [26]), as observed in previous studies [39,40]. Our experiment indicates that the absorbed atom can repair the Se vacancy of the substrate (see Fig. S7 in the SM [26]), which help us to demonstrate explicitly that the chemisorbed atom is the Se atom at the interface. The chemisorbed Se and Se vacancy can generate strong intervalley scattering in graphene, characterized as a threefold $\sqrt{3}\times\sqrt{3}$ pattern that is rotated 30° with respect to the graphene lattice, as shown in Fig. 1(b). In our experiment, the Se atoms usually travel about 2 nm, specifically, 14.15 nm at maximum and 0.293 nm at minimum, from the Se vacancy at the interface upon a pulse.

The chemisorbed Se atoms at the interface exhibit two kinds of distinct features in the STM images, as shown in Figs. 1(d) and 1(h). The most common case is that a pair of the nearest C atoms becomes the highest positions in the STM image and the induced intervalley scattering exhibits a mirror symmetry with respect to the C-C bond [Fig. 1(d)]. Such characteristic features are similar to that of a nitrogen atom chemisorbed on a C-C bond in graphene [41] and the observed pattern is attributed to the chemisorption of an individual Se atom at the bridge site in graphene. Since there are three directions of the C-C bonds in graphene, we observe three directions of such pattern (see Fig. S1(b) in the SM [26]). The other case, as depicted in Fig. 1(h), has a threefold symmetry with the highest site localized at the center of a C atom in graphene. This feature is similar to that of a single atom absorbed on a C atom in graphene [7,9,10] and the observed pattern is associated with the chemisorption of an individual Se atom on the graphene sublattice. In our STM measurements, the moiré pattern generated between graphene and the $WSe_2$ substrate will break the $C_3$ symmetry of the chemisorbed Se atom on a C site in graphene. However, it is unlikely to significantly affect the electronic properties of the on-site chemisorbed Se atom due to the weak vdW interaction between graphene and the $WSe_2$ [16,42–46], as demonstrated subsequently. To gain deep insight, we carry out simulations on a single Se atom chemisorbed on graphene at the bridge and C atom sites. The local atomic structures in

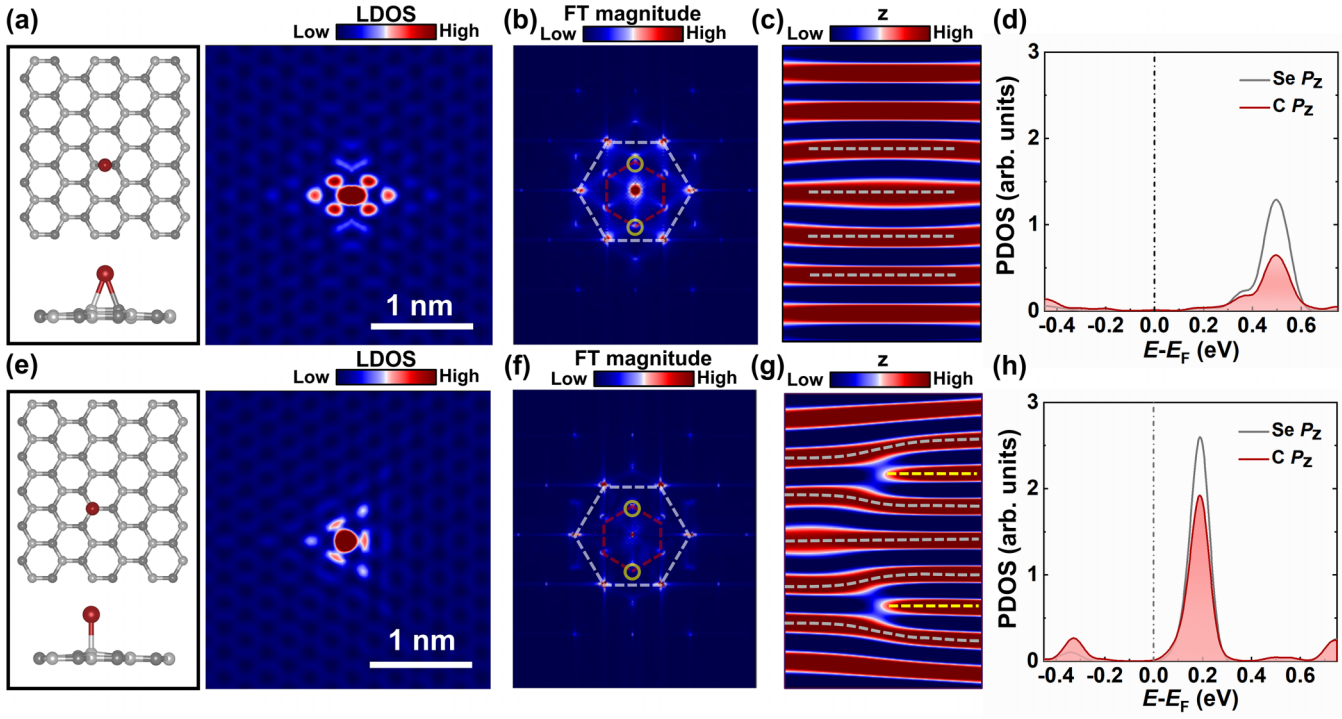


FIG. 2. (a), (e) Optimized atomic geometries (left panels) and LDOS (right panels) of a Se adatom at the C-C bridge and the C atom of the surface of graphene, respectively. (b), (f) The FT images of the LDOS. The outer hexangular spots and inner bright spots correspond to the reciprocal lattice of graphene and the interference of the intervalley scattering, respectively. (c), (g) FT-filtered images enclosed by yellow circles in (b), (f). (d), (h) The projected DOS on the Se atom and C atoms near the chemisorbed Se.

both cases exhibit the out of plane buckling of the C atoms around the chemisorbed Se atom, as shown in Figs. 2(a) and 2(e). Obviously, the simulated local density of states (LDOS) for the C-C bridge at 0.35 eV and the C site at 0.2 eV are in good agreement with that measured in experiments (the topography images in Fig. 1 are measured at very low bias and mainly reflect the spatial distribution of the LDOS). Our theoretical calculations also reveal that the most stable state is the Se at the bridge site with the binding energy of ∼1.02 eV, and it costs a modest energy expense of 0.17 eV when the Se is at the C site. This is in line with the experiments: for 90 well-characterized chemisorbed atoms, 36 Se atoms are chemisorbed at the C atom and 54 Se atoms are chemisorbed under the C-C bond.

The chemisorbed Se atom is expected to generate localized electronic states near the Fermi level ($E_F$) in graphene. Figures 1(g) and 1(k) show spatially resolved STS contour plots along the yellow arrows in Figs. 1(b) and 1(h), respectively. Apparently, the $dI/dV$ spectra exhibit a peak at 280 meV when the Se atom is chemisorbed at the C-C bridge and they display a peak at 180 meV when the Se atom is chemisorbed on the C atom. The localized states extend several nanometers away from the chemisorbed Se atom and the weaker peaks in the spectra recorded away from the chemisorbed Se atom are attributed to tip-induced quasibound states in graphene, as observed previously [47,48]. To understand the origin of the localized states, we analyze the low-energy projected DOS (PDOS) for the two adsorption sites, as shown in Figs. 2(d) and 2(h), respectively. A peak originated from the hybridization between Se-$p_z$ and C-$p_z$ orbitals is observed at 500 meV for the ground state, and a similar peak appears at 200 meV when the Se atom is chemisorbed on the C site, which is qualitatively in line with our experimental results (see Fig. S5 in the SM [26]). The concentration of the chemisorbed Se atoms in the simulations is greater than that in the experiments, which may cause the higher energy of the peaks seen in the theoretical calculations (see Fig. S13 in the SM [26]). The neglect of the tip in theory may also partially contribute to the difference. Although all the chemisorbed Se atoms can generate strong intervalley scattering in graphene, as shown in both STM images [Figs. 1(d) and 1(h)] and their Fourier transform (FT) images [Figs. 1(e) and 1(i)], the induced intervalley scatterings exhibit distinct pseudospin-mediated physics. Figures 1(f) and 1(j) show inverse FT-filtered images for two different Se adsorption sites, which exhibit different characteristics (see Fig. S4 for more experimental results [26]). No dislocation ($|N| = 0$) is observed in the vicinity of the Se atom adsorbed at the C-C bridge in graphene, whereas two additional wavefront dislocations ($|N| = 2$) appear when the Se atom is chemisorbed on the C site. The chemisorbed Se atom will introduce both intravalley scattering and intervalley scattering in graphene [16–18], as schematically shown in Fig. 1(c). The intravalley scattering involves a rotation of the momentum-locked pseudospin that is always $\pi$. Thus the interference is counterbalanced at the leading order. In contrast, the intervalley backscattering involves a rotation of the pseudospin by an angle $-2\theta_q = -2\theta_r$. An accumulation of the phase shift over a closed path enclosing the single atomic defect is $\pm \int_0^{2\pi} 2d\theta_q = \pm 4\pi$. Motivated by this, the Se atom adsorbed at the graphene A (B) sublattice can be regarded as a pseudospin-mediated atomic-scale vortex, which is located at the absorbed position, with angular mo-

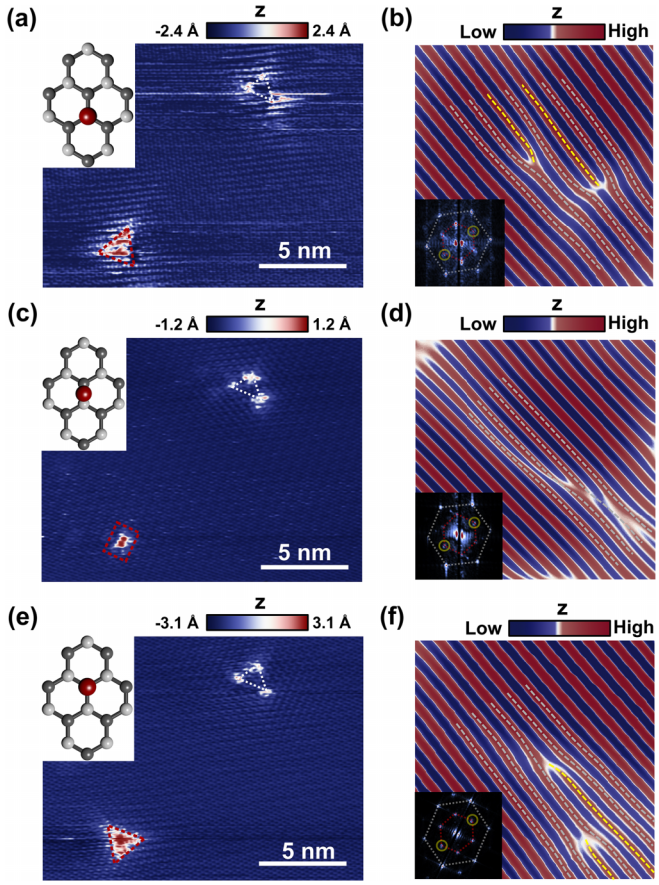


FIG. 3. (a), (c), (e) STM images of a single Se adatom chemisorbed on the A sublattice, C-C bridge, and B sublattice of graphene, respectively. The defect, as marked with dotted white lines, is used as a reference object. The schematic atomic structures are given in the insets. (b), (d), (f) FT-filtered images near the Se adatom shown in (a), (c), (e) along the marked pair of signatures of intervalley scatterings. Insets: FT of the STM images. Graphene and intervalley scattering Bragg peaks are connected with white and red dotted lines, respectively.

menta $l = +2$ ($l = -2$), reflecting the Berry phase in the monolayer graphene [16–18]. Meanwhile, the angular momentum of the Se atom chemisorbed at the C-C bridge is $l = +2 + (-2) = 0$, because the Se atom establishes bonds with two C atoms which belong to the A and B sublattice, respectively. The FT-filtered STM images reflect the interference patterns of a uniform plane wave and a defect-induced atomic-scale vortex. Therefore, the total number of additional wavefronts reflects the angular momentum of the vortex. The above analysis is further confirmed by the first-principles calculations. The FT from the simulated LDOS in Figs. 2(a) and 2(e) also shows signals of the intervalley scattering [see Figs. 2(b) and 2(f)]. Furthermore, the FT-filtered images, as shown in Figs. 2(c) and 2(g), have the same number of corresponding additional wavefront dislocations as that in the experiments (see the method section and the SM for computational details [26]). Both our experiments and theoretical calculations indicate that a Se atom chemisorbed at two different sites in graphene can introduce different electronic properties.

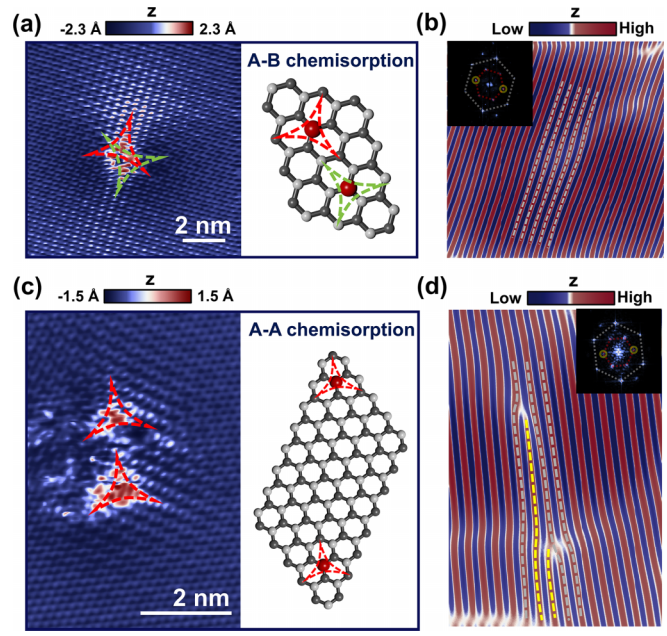


FIG. 4. Interference of pseudospin-mediated vortices and wavefront dislocations induced by A-B chemisorption and A-A chemisorption. (a), (c) Typical STM images of two individual Se adatoms chemisorbed on different or the same sublattices of graphene, respectively. The right panels present the corresponding atomic structures of the Se atoms absorbed on graphene. (b), (d) FT-filtered images in (a), (c) along the marked reciprocal lattice points. Insets: the filters applied in the Fourier space. White and red dotted lines connect the graphene and intervalley scattering Bragg peaks, respectively.

Besides *in situ* creating of chemisorbed individual Se atoms on graphene, our experiment further realizes precise manipulation of the chemisorption positions and chemical bonds between the Se and graphene using the STM tip. Figure 3 summarizes a representative example (see more details in the SM [26]). As shown in Figs. 3(a), 3(c), and 3(e), our experiment demonstrates explicitly that we can tune the chemisorbed positions and bond between the Se atom and graphene. In Figs. 3(a) and 3(e), the Se atom is chemisorbed on the A sublattice and B sublattice, respectively, which can be identified according to the Se-induced tripod shapes. In Fig. 3(c), the Se atom is chemisorbed on the C-C bridge, exhibiting the same features shown in Fig. 1(d) and Fig. 2(a). The tunable chemisorbed positions and bond change the pseudospin-mediated intervalley scattering around the Se atom. Figures 3(b), 3(d), and 3(f) show the corresponding FT-filtered images, where the $N = 2, 0, -2$ additional wavefront dislocations are obtained in the vicinity of the chemisorbed Se atom, respectively (see Fig. S6 for the original STM images [26]), indicating the variation of angular momenta $l = +2$, $l = 0, l = -2$ of the pseudospin-mediated vortices. According to previous studies [7–9,11–14], tuning the C-$p_z$ peaks to the $E_F$ will cause a spin splitting and result in a local magnetic moment in graphene, and such spin state can be manipulated by the local field [49]. Thus the system is potentially spin polarized with the Se atom chemisorbed under the C sublattice when the localized C-$p_z$ state, i.e., the peak at 0.2 eV above

the $E_F$, is gated near the $E_F$. When placing a charge sphere $1e^-$ as a local gate on the top of graphene with a Se atom, such a system turns out to be magnetic with a spin moment of 0.5 $\mu_B$ (see Fig. S17 in the SM [26]). Therefore, it is possibly to tune both pseudospin-mediated and spin-related properties in graphene by manipulating the chemisorption sites of individual Se atoms and the filling of the localized states of adsorbed Se atoms.

With the ability to control the chemical reaction between the individual Se atom and graphene with atomic-level precision, then, it becomes possible to combine different kinds of chemisorbed Se atoms to further tune properties of graphene. Figure 4 summarizes two representative results that two individual Se atoms are chemisorbed at opposite (AB chemisorption) or the same sublattices (AA chemisorption) in graphene (see Figs. S8 and S10 for more experimental results [26]). For the case of the AB chemisorption [Fig. 4(a)], there is zero additional wavefront dislocation, as shown in Fig. 4(b), resulting from the annihilation of dislocations of the pseudospin-mediated vortices with opposite angular momenta. For the case of the AA chemisorption [Fig. 4(c)], the number of additional wavefronts induced by the two A-site adsorptions is still 2 [Fig. 4(d)]. Such a counterintuitive result can be well explained with considering the interference of two pseudospin-mediated vortices [17]. The winding number of the pseudospin over a closed path surrounding two $l = +2$ vortices is still 2; consequently, we obtain $|N| = 2$ additional wavefronts. If further considering the fact that individual atoms chemisorbed on A and B sublattices of graphene with gating will result in local magnetic moments in opposite directions [7,50–52], it would be expected to obtain completely different magnetic coupling between the local magnetic moments for the AB and AA chemisorptions. By using our method, as shown in Fig. S9 [26], it is possible to realize large-area chemisorption of the Se atoms only on the A (or B) sublattice and to explore the possibility of 100% spin polarization in graphene in the near future.

In summary, we demonstrate the ability to extract individual Se atoms and the manipulation of its chemisorption on graphene with atomic-level precision. By manipulating the adsorption sites of individual Se atoms, our results indicate that we can introduce distinct pseudospin-mediated atomic-scale vortices in graphene and explore their quantum interference. The reported *ab initio* approach combines the high spatial resolution of the STM technique and the highly tunable chemical bonding between individual Se atoms and graphene. Our study lays a solid foundation for realizing custom-designed future materials through atomic-level precise chemical doping.

This work was supported by the National Key R and D Program of China (Grants No. 2021YFA1401900 and No. 2021YFA1400100), the National Natural Science Foundation of China (Grants No.12141401, No. 11974050, No.11934003, and No. U1930402), "the Fundamental Research Funds for the Central Universities" (Grant No. 310400209521), Grant TED2021-132388B-C44 funded by MCIN/AEI/10.13039/501100011033 and Unión Europea Next Generation EU/PRTR and Grant PID2022-140845OB-C66 funded by MCIN/AEI/10.13039/501100011033 and FEDER Una manera de hacer Europa and the China Postdoctoral Science Foundation (Grant No. 2023M740296). F.G. and M.B. acknowledge support from Villum fonden (Project No. VIL13340), and A.B.L. acknowledges support from the Independent Research Fund Denmark (Project No. 0135-00372A).

[1] C. Tan, X. Cao, X.-J. Wu, Q. He, J. Yang, X. Zhang, J. Chen, W. Zhao, S. Han, G.-H. Nam *et al.*, Recent advances in ultrathin two-dimensional nanomaterials, Chem. Rev. **117**, 6225 (2017).

[2] P. Luo, F. Zhuge, Q. Zhang, Y. Chen, L. Lv, Y. Huang, H. Li, and T. Zhai, Doping engineering and functionalization of two-dimensional metal chalcogenides, Nanoscale Horiz. **4**, 26 (2019).

[3] A. H. Castro Neto, F. Guinea, N. M. R. Peres, K. S. Novoselov, and A. K. Geim, The electronic properties of graphene, Rev. Mod. Phys. **81**, 109 (2009).

[4] H. Liu, Y. Liu, and D. Zhu, Chemical doping of graphene, J. Mater. Chem. **21**, 3335 (2011).

[5] H. Wang, T. Maiyalagan, and X. Wang, Review on recent progress in nitrogen-doped graphene: Synthesis, characterization, and its potential applications, ACS Catal. **2**, 781 (2012).

[6] X. Wang, X. Li, L. Zhang, Y. Yoon, P. K. Weber, H. Wang, J. Guo, and H. Dai, N-doping of graphene through electrothermal reactions with ammonia, Science **324**, 768 (2009).

[7] H. Gonzalez-Herrero, J. M. Gomez-Rodriguez, P. Mallet, M. Moaied, J. Jose Palacios, C. Salgado, M. M. Ugeda, J.-Y. Veuillen, F. Yndurain, and I. Brihuega, Atomic-scale control of graphene magnetism by using hydrogen atoms, Science **352**, 437 (2016).

[8] Y. Zhang, S.-Y. Li, H. Huang, W.-T. Li, J.-B. Qiao, W.-X. Wang, L.-J. Yin, K.-K. Bai, W. Duan, and L. He, Scanning tunneling microscopy of the $\pi$ magnetism of a single carbon vacancy in graphene, Phys. Rev. Lett. **117**, 166801 (2016).

[9] Y. Zhang, F. Gao, S. Gao, and L. He, Tunable magnetism of a single-carbon vacancy in graphene, Sci. Bull. **65**, 194 (2020).

[10] G. M. Rutter, J. N. Crain, N. P. Guisinger, T. Li, P. N. First, and J. A. Stroscio, Scattering and interference in epitaxial graphene, Science **317**, 219 (2007).

[11] M. M. Ugeda, I. Brihuega, F. Guinea, and J. M. Gomez-Rodriguez, Missing atom as a source of carbon magnetism, Phys. Rev. Lett. **104**, 096804 (2010).

[12] R. R. Nair, M. Sepioni, I. L. Tsai, O. Lehtinen, J. Keinonen, A. V. Krasheninnikov, T. Thomson, A. K. Geim, and I. V. Grigorieva, Spin-half paramagnetism in graphene induced by point defects, Nat. Phys. **8**, 199 (2012).

[13] M. M. Ugeda, D. Fernandez-Torre, I. Brihuega, P. Pou, A. J. Martinez-Galera, R. Perez, and J. M. Gomez-Rodriguez, Point defects on graphene on metals, Phys. Rev. Lett. **107**, 116803 (2011).

[14] J.-H. Chen, L. Li, W. G. Cullen, E. D. Williams, and M. S. Fuhrer, Tunable Kondo effect in graphene with defects, Nat. Phys. **7**, 535 (2011).

[15] Y. Jiang, P.-W. Lo, D. May, G. Li, G.-Y. Guo, F. B. Anders, T. Taniguchi, K. Watanabe, J. Mao, and E. Y. Andrei, Inducing Kondo screening of vacancy magnetic moments in graphene with gating and local curvature, Nat. Commun. **9**, 2349 (2018).

[16] C. Dutreix, H. Gonzalez-Herrero, I. Brihuega, M. I. Katsnelson, C. Chapelier, and V. T. Renard, Measuring the Berry phase of graphene from wavefront dislocations in Friedel oscillations, Nature (London) **574**, 219 (2019).

[17] Y. Zhang, Y. Su, and L. He, Quantum interferences of pseudospin-mediated atomic-scale vortices in monolayer graphene, Nano Lett. **21**, 2526 (2021).

[18] Y. Zhang, Y. Su, and L. He, Local Berry phase signatures of bilayer graphene in intervalley quantum interference, Phys. Rev. Lett. **125**, 116804 (2020).

[19] Y. Zhang, F. Gao, S. Gao, M. Brandbyge, and L. He, Characterization and manipulation of intervalley scattering induced by an individual monovacancy in graphene, Phys. Rev. Lett. **129**, 096402 (2022).

[20] L. Sha, P. Gao, X. Ren, Q. Chi, Y. Chen, and P. Yang, A Self-repairing cathode material for lithium-selenium batteries: Se-C chemically bonded selenium-graphene composite, Chemistry **24**, 2151 (2018).

[21] A. W. Robertson, C. S. Allen, Y. A. Wu, K. He, J. Olivier, J. Neethling, A. I. Kirkland, and J. H. Warner, Spatial control of defect creation in graphene at the nanoscale, Nat. Commun. **3**, 2141 (2012).

[22] P.-C. Lin, R. Villarreal, S. Achilli, H. Bana, M. N. Nair, A. Tejeda, K. Verguts, S. De Gendt, M. Auge, H. Hofsäss *et al.*, Doping graphene with substitutional Mn, ACS Nano **15**, 5449 (2021).

[23] F. Zeng, W.-B. Zhang, and B.-Y. Tang, Electronic structures and elastic properties of monolayer and bilayer transition metal dichalcogenides $MX_2$ ($M$ = Mo, W; $X$ = O, S, Se, Te): A comparative first-principles study, Chin. Phys. B **24**, 097103 (2015).

[24] D. Wong, J. Velasco, L. Ju, J. Lee, S. Kahn, H.-Z. Tsai, C. Germany, T. Taniguchi, K. Watanabe, A. Zettl *et al.*, Characterization and manipulation of individual defects in insulating hexagonal boron nitride using scanning tunnelling microscopy, Nat. Nanotechnol. **10**, 949 (2015).

[25] W.-X. Wang, Y.-W. Wei, S.-Y. Li, X. Li, X. Wu, J. Feng, and L. He, Imaging the dynamics of an individual hydrogen atom intercalated between two graphene sheets, Phys. Rev. B **97**, 085407 (2018).

[26] See Supplemental Material at http://link.aps.org/supplemental/10.1103/PhysRevB.110.L041405 for sample preparation, more experimental data, details of calculation, and discussion, which includes Refs. [27–38].

[27] J. P. Perdew, K. Burke, and M. Ernzerhof, Generalized gradient approximation made simple, Phys. Rev. Lett. **77**, 3865 (1996).

[28] M. Brandbyge, J. L. Mozos, P. Ordejón, J. Taylor, and K. Stokbro, Density-functional method for nonequilibrium electron transport, Phys. Rev. B **65**, 165401 (2002).

[29] J. M. Soler, E. Artacho, J. D. Gale, A. García, J. Junquera, P. Ordejón, and D. Sánchez-Portal, The SIESTA method for *ab initio* order-$N$ materials simulation, J. Phys.: Condens. Matter. **14**, 2745 (2002).

[30] N. Papior, N. Lorente, T. Frederiksen, A. Garcia, and M. Brandbyge, Improvements on non-equilibrium and transport Green function techniques: The next-generation transiesta, Comput. Phys. Commun. **212**, 8 (2017).

[31] G. Kresse and J. Hafner, *Ab initio* molecular dynamics for liquid metals, Phys. Rev. B **47**, 558 (1993).

[32] N. Papior, G. Calogero, S. Leitherer, and M. Brandbyge, Removing all periodic boundary conditions: Efficient nonequilibrium Green's function calculations, Phys. Rev. B **100**, 195417 (2019).

[33] G. Calogero, N. Papior, M. Koleini, M. H. L. Larsen, and M. Brandbyge, Multi-scale approach to first-principles electron transport beyond 100 nm, Nanoscale **11**, 6153 (2019).

[34] N. Papior, sisl: v0.10.0 (2020), https://doi.org/10.5281/zenodo.597181.

[35] D. Vanderbilt, Soft self-consistent pseudopotentials in a generalized eigenvalue formalism, Phys. Rev. B **41**, 7892 (1990).

[36] P. E. Blochl, Projector augmented-wave method, Phys. Rev. B **50**, 17953 (1994).

[37] Y. Wang and J. P. Perdew, Correlation hole of the spin-polarized electron gas, with exact small-wave-vector and high-density scaling, Phys. Rev. B **44**, 13298 (1991).

[38] M. Sun, J.-P. Chou, J. Yu, and W. Tang, Effects of structural imperfection on the electronic properties of graphene/$WSe_2$ heterostructures, J. Mater. Chem. C **5**, 10383 (2017).

[39] J. Shim, H. S. Kim, Y. S. Shim, D.-H. Kang, H.-Y. Park, J. Lee, J. Jeon, S. J. Jung, Y. J. Song, W.-S. Jung *et al.*, Extremely large gate modulation in vertical graphene/$WSe_2$ heterojunction barristor based on a novel transport mechanism, Adv. Mater. **28**, 5293 (2016).

[40] T. D. Nguyen, J. Jiang, B. Song, M. D. Tran, W. Choi, J. H. Kim, Y. M. Kim, D. L. Duong, and Y. H. Lee, Gate-tunable magnetism via resonant Se-vacancy levels in $WSe_2$, Adv. Sci. **8**, 202102911 (2021).

[41] Y. Tison, J. Lagoute, V. Repain, C. Chacon, Y. Girard, S. Rousset, F. Joucken, D. Sharma, L. Henrard, H. Amara *et al.*, Electronic interaction between nitrogen atoms in doped graphene, ACS Nano **9**, 670 (2015).

[42] Y.-W. Liu, Y.-C. Zhuang, Y.-N. Ren, C. Yan, X.-F. Zhou, Q. Yang, Q.-F. Sun, and L. He, Visualizing a single wavefront dislocation induced by orbital angular momentum in graphene, Nat. Commun. **15**, 3546 (2024).

[43] W. H. Blades, N. J. Frady, P. M. Litwin, S. J. McDonnell, and P. Reinke, Thermally induced defects on $WSe_2$, J. Phys. Chem. C **124**, 15337 (2020).

[44] C. J. Arguello, S. P. Chockalingam, E. P. Rosenthal, L. Zhao, C. Gutiérrez, J. H. Kang, W. C. Chung, R. M. Fernandes, S. Jia, A. J. Millis *et al.*, Visualizing the charge density wave transition in $2H$-$NbSe_2$ in real space, Phys. Rev. B **89**, 235115 (2014).

[45] M. Gmitra, D. Kochan, P. Hoegl, and J. Fabian, Trivial and inverted Dirac bands and the emergence of quantum spin Hall states in graphene on transition-metal dichalcogenides, Phys. Rev. B **93**, 155104 (2016).

[46] A. M. Alsharari, M. M. Asmar, and S. E. Ulloa, Topological phases and twisting of graphene on a dichalcogenide monolayer, Phys. Rev. B **98**, 195129 (2018).

[47] Y. Zhao, J. Wyrick, F. D. Natterer, J. F. Rodriguez-Nieva, C. Lewandowski, K. Watanabe, T. Taniguchi, L. S. Levitov, N. B. Zhitenev, and J. A. Stroscio, Creating and probing electron whispering-gallery modes in graphene, Science **348**, 672 (2015).

[48] Y.-N. Ren, Q. Cheng, S.-Y. Li, C. Yan, Y.-W. Liu, K. Lv, M.-H. Zhang, Q.-F. Sun, and L. He, Spatial and magnetic confinement of massless Dirac fermions, Phy. Rev. B **104**, L161408 (2021).

[49] F. Gao, Y. Zhang, L. He, S. Gao, and M. Brandbyge, Control of the local magnetic states in graphene with voltage and gating, Phys. Rev. B **103**, L241402 (2021).

[50] O. V. Yazyev, Magnetism in disordered graphene and irradiated graphite, Phys. Rev. Lett. **101**, 037203 (2008).

[51] W. Han, R. K. Kawakami, M. Gmitra, and J. Fabian, Graphene spintronics, Nat. Nanotechnol. **9**, 794 (2014).

[52] D. Pesin and A. H. MacDonald, Spintronics and pseudospintronics in graphene and topological insulators, Nat. Mater. **11**, 409 (2012).